Intersubunit Salt Bridges with a Sulfate Anion Control Subunit Dissociation and Thermal Stabilization of Bacillus sp. TB-90 Urate Oxidase

ARTICLE *in* BIOCHEMISTRY · JUNE 2014

Impact Factor: 3.02 · DOI: 10.1021/bi500137b · Source: PubMed

6 AUTHORS, INCLUDING:

Takao Hibi
Fukui Prefectural University
41 PUBLICATIONS **364** CITATIONS
SEE PROFILE

Takafumi Itoh
Fukui Prefectural University
39 PUBLICATIONS **372** CITATIONS
SEE PROFILE

BIOCHEMISTRY
including biophysical chemistry & molecular biology

Article

pubs.acs.org/biochemistry

Intersubunit Salt Bridges with a Sulfate Anion Control Subunit Dissociation and Thermal Stabilization of *Bacillus* sp. TB-90 Urate Oxidase

Takao Hibi,*[,†] Yuta Hayashi,[†] Harumi Fukada,[§] Takafumi Itoh,[†] Tomohiro Nago,[†,∥] and Yoshiaki Nishiya[‡,⊥]

[†]Department of Bioscience, Fukui Prefectural University, Eiheiji City, Yoshida District, Fukui 910-1195, Japan

[‡]Tsuruga Institute of Biotechnology, Toyobo Company Ltd., Tsuruga, Fukui 914-0047, Japan

[§]Graduate School of Life and Environmental Sciences, Osaka Prefecture University, Sakai, Osaka 599-8531, Japan

ABSTRACT: The optimal activity of *Bacillus* sp. TB-90 urate oxidase (BTUO) is 45 °C, but this enzyme is one of the most thermostable urate oxidases. A marked increase (>10 °C) in its thermal stability is induced by high concentrations (0.8−1.2 M) of sodium sulfate. Calorimetric measurements and size exclusion chromatographic analyses suggested that sulfate-induced thermal stabilization is related to the binding of a sulfate anion that repressed the dissociation of BTUO tetramers into dimers. To determine the sulfate binding site, the crystal structure was determined at 1.75 Å resolution. The bound sulfate anion was found at the subunit interface of the symmetrical related subunits and formed a salt bridge with two Arg298 residues in the flexible loop that is involved in subunit assembly. Site-directed mutagenesis of Arg298 to Glu was used to extensively characterize the sulfate binding site at the subunit interface. The network of charged hydrogen bonds via the bound sulfate is suggested to contribute significantly to the thermal stabilization of both subunit dimers and the tetrameric assembly of BTUO. Knowledge of the mechanism of salt-induced stabilization will help to develop new strategies for enhancing protein thermal stabilization.

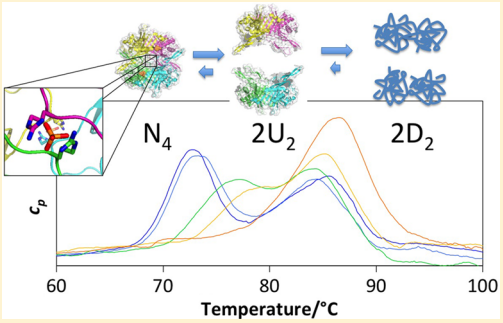

Urate oxidases catalyze the oxidative opening of the urate purine ring to yield 5-hydroxyisourea, CO_2, and H_2O_2. This enzyme is crucial for determining uric acid levels in biological fluids for diagnosis of hyperuricemia, because the highly specific reaction of urate oxidase allows the simple colorimetric detection of uric acid. The thermal, chemical, and long-term stability of urate oxidase plays a critical role in its application to enzymatic analysis[1] and medical treatment[2] for hyperuricemia and gout. Although it is essentially expected to be thermally stable for these applications, to date genes encoding urate oxidase have been found in only one hyperthermophilic organism, *Geobacillus thermocatenulatus*.[3] Several different methods can be used to modulate the enzyme stability, including enzyme immobilization,[4] chemical modification,[5] and encapsulation in lipid vesicles.[6] Urate oxidase from *Bacillus* sp. TB-90 (BTUO; urate:oxygen oxidoreductase), which is genetically encoded by a fusion gene with a 2-oxo-4-hydroxy-4-carboxy-5-ureidoimidazoline decarboxylase domain,[7] is secreted as a tetrameric protein of identical subunits (331 residues per subunit, molecular mass of 37863.8 Da × 4).[8,9] With an optimal activity at 45 °C and a transition temperature at which the enzyme retains 50% of its initial activity at 65 °C, BTUO is one of the most thermostable urate oxidases.[9] We recently found that the thermal stability of BTUO was remarkably enhanced in the presence of a high concentration of sulfate salt, and such enhancement of thermal stabilization of a urate oxidase has not been seen previously.

Here we characterized the thermal stabilization of BTUO induced by sulfate binding, using several analytical methods, including a thermal shift assay, differential scanning calorimetry (DSC), and size exclusion chromatography (SEC). The crystal structure of the enzyme was previously determined in the presence of Li_2SO_4 (PDB entry 1J2G). Although Li_2SO_4 showed an only minor effect on the salt-induced thermal stabilization probably because of the destabilizing effect of lithium ion,[10] four sulfates per tetramer molecule were bound to the enzyme surface. In this study, the crystal structure with K_2SO_4, a potent salt in the thermal stabilization as well as Na_2SO_4, was determined at 1.75 Å resolution. This structure showed a single bound sulfate that participated in the formation of salt bridges via two Arg298 residues located at the subunit interface rather than the active site. Site-directed mutagenesis of this Arg298 residue was also conducted to investigate the role of the sulfate binding site in thermal stabilization. These results revealed a novel mechanism for the thermal stabilization of the macromolecule through the binding of a sulfate at the subunit interface.

Received: January 31, 2014
Revised: June 2, 2014
Published: June 4, 2014

   dx.doi.org/10.1021/bi500137b | *Biochemistry* 2014, 53, 3879−3888

EXPERIMENTAL PROCEDURES

Materials. Recombinant BTUO was overexpressed in *Escherichia coli* strain DH5α and purified as described previously.[9] The enzyme purity and homogeneity were assessed by sodium dodecyl sulfate−polyacrylamide gel electrophoresis (SDS−PAGE) and dynamic light scattering analysis. To determine the BTUO concentration spectrophotometrically, we calculated a molar extinction coefficient at 280 nm of $(1.39 \pm 0.01) \times 10^5$ M^{-1} cm^{-1} using the Edelhoch method.[11,12]

Thermal Shift Assay. Thermal shift assays were conducted using the Applied Biosystems StepOne system (Life Technologies Co. Ltd.). Protein/salt solutions (20 μL) containing 1 mg/mL BTUO and ROX dye were dispensed into a MicroAmp Optical Reaction 48-well microplate (Life Technologies Co. Ltd.), and the plate was sealed with an optical adhesive film to prevent evaporation. The plate was set into the StepOne instrument and heated from 20 to 99 °C at a rate of 0.8 K/min for all experiments. Fluorescence emissions above 610 nm were detected. To approximate the temperature midpoint for the protein denaturation transition, T_d, fluorescence intensity data at T, $y(T)$, were fit to a Boltzmann model, shown in eq 1,[13] using Origin (OriginLab Co. Ltd.):

$$y(T) = y_F + \frac{y_U - y_F}{1 + e^{(T_d - T)/a}} \quad (1)$$

where y_F and y_U are pretransitional and post-transitional fluorescence intensities, respectively, and α is the slope factor.

Enzyme Assay. Urate oxidase was assayed by following the disappearance of uric acid, as detected by a decrease in absorbance at 291 nm in the presence of the enzyme. The assay mixture contained 0.05 mL of the enzyme solution [50 mM borate buffer (pH 8.5) with 50 mM potassium chloride] and 120 μM uric acid in a final volume of 2.0 mL. The unit of activity was defined as the amount of enzyme that catalyzed the transformation of 1 μmol of substrate/min at 37 °C and pH 8.5. The extinction coefficient for uric acid was assumed to be 1.22×10^4 M^{-1} cm^{-1}.[14]

Calorimetric Measurement. Calorimetric measurements were performed by differential microcalorimetry using a nanoDSC differential scanning microcalorimeter (Calorimetry Sciences Corp.).[15] The experiments were conducted between 20 and 100 °C at a scan rate of 1 K/min. The protein solutions were dialyzed against 50 mM borate buffer (pH 8.5), and the dialysis buffer was used as a reference. The baseline for each run was determined in an identical experiment with buffer in both cells. To prevent the formation of bubbles during heating, the samples and reference solutions were degassed while being gently stirred at room temperature under vacuum before being loaded into the cells.

DSC curves were analyzed in terms of an approximate model of two-state denaturation with self-dissociation.[16] The statistics of the fit were calculated using Origin (OriginLab Co. Ltd.) and the assumption that the denaturation process can be considered to take place in three sequential steps:

$$N_4 \rightleftarrows 2U_2 \rightleftarrows 2D_2 \quad (2)$$

where N_4 is the native form of the BTUO tetramer, U_2 is the partially unfolded dimer, and D_2 is the final denatured state.

Size Exclusion Chromatography (SEC). The BTUO subunit composition was obtained using SEC. Small particulates were removed from each sample by filtration with a Cosmospin Filter G (pore size of 0.2 μm, Nacalai Tesque Inc.). A 2.0 mm × 30 cm TSK-GEL Super SW3000 column (Tosoh Bioscience) was mounted on a TOSOH high-performance liquid chromatography instrument. Analyses were performed in isocratic mode using 50 mM sodium phosphate buffer (pH 7.0) and 150 mM NaCl at a flow rate of 0.065 mL/min unless otherwise noted. The absorbance at 280 nm was recorded.

For a self-dissociation system of BTUO, the dissociation reaction is depicted in the scheme below:

$$N_4 \underset{K_d}{\rightleftarrows} N_2 + N_2 \quad (3)$$

The dissociation constant, K_d, is defined by

$$K_d = \frac{[N_2]^2}{[N_4]}$$

The degree of association, Z, is defined by

$$Z = \frac{[N_4]}{[N_4] + \frac{1}{2}[N_2]}$$

which can be calculated from the peak areas of tetramer N_4 and dimer N_2.

Solving the preceding equation for $[N_4]$ gives eq 4

$$\frac{Z}{\sqrt{[N_4]}} = \frac{Z}{\sqrt{K_d}}(1 - Z) \quad (4)$$

To investigate the changes in K_d upon addition of Na_2SO_4, the statistics of the fit are calculated using eq 4. In the presence of excess Na_2SO_4, the dissociation reaction is assumed to proceed according to the following equation:

$$N_4\text{-}2SO_4^{2-} \underset{K_d}{\rightleftarrows} N_2 + N_2 + 2SO_4^{2-} \quad (3')$$

Protein Crystallization and Data Collection. To obtain high-quality crystals, the 6 (TKHKER) and 13 (MFSDEPDHKGALK) N- and C-terminal residues, respectively, were deleted from wild-type BTUO. The deleted N-terminal region was disordered in the 2.2 Å crystal structure (PDB entry 1J2G), and the C-terminal region was processed in the *Bacillus* but not *E. coli* expression systems.[9] The expressed enzyme was purified as previously described.[9] BTUO crystals were grown by the hanging-drop vapor-diffusion technique, wherein a protein solution (2 μL) was mixed with an equal volume of reservoir solution containing 15% (w/v) PEG 8000, 100 mM Tris-HCl (pH 8.0), 0.07 M K_2SO_4, and 2 mM 8-azaxanthine. A native data set was collected to 1.75 Å resolution using one crystal. The resulting crystal was momentarily soaked in the reservoir solution containing 20% 2-ethoxyethanol, flash-cooled in a 100 K dry nitrogen stream, and then exposed to 1 Å X-ray beam at 100 K.

X-ray diffraction data for the wild-type crystal were collected using an ADSC Quantum 210 CCD camera and synchrotron radiation on beamline NW12A (Photon Factory, Tsukuba, Japan). Individual frames consisted of a 0.5° oscillation angle measured for 5 s at a crystal-to-detector distance of 117.1 mm. The crystal belonged to orthorhombic space group $P2_12_12$ with the following unit cell dimensions: a = 133.57 Å, b = 144.64 Å, and c = 70.79 Å. Intensity data were processed, merged, and scaled with HKL2000.[17] Data collection statistics are listed in Table 1. A 99.8% complete data set from the crystal was processed to 1.75 Å, with an overall R_{merge} of 9.4%, and 1884330 total reflections, including 138568 unique reflections. Assuming four subunits (molecular mass of 36236.9 × 4) per

dx.doi.org/10.1021/bi500137b | *Biochemistry* 2014, 53, 3879−3888

Table 1. Data Collection and Refinement Statistics

Data Collection[a]	
space group	$P2_12_12$
unit cell parameters (Å)	a = 133.57, b = 144.64, c = 70.79
resolution range (Å)	30−1.75 (1.78−1.75)
total no. of reflections	1884330
no. of unique reflections	138568
completeness (%)	99.8 (100.0)
R_{merge} ($=\sum_h\sum_i\lvert I_{h,i} - \langle I_h\rangle\rvert/\sum_h\sum_i\lvert I_{h,i}\rvert$)	0.094 (0.377)
I/σ	56.8 (9.4)
redundancy	13.6 (13.0)
Wilson B factor (Å^2)	27.2
Refinement	
refinement resolution (Å)	19.92−1.75
no. of reflections (work/free)	126254/6672
no. of protein atoms	9830 (A, 2437; B, 2477; C, 2466; D, 2450)
no. of ligand atoms	16
no. of water molecules	1015
missing residues	311−324
R_{work}/R_{free}	0.159/0.190
rmsd	
bond lengths (Å)	0.010
bond angles (deg)	1.28
mean B factor (Å^2)	
main chain atoms	18.40 (A, 18.94; B, 17.85; C, 18.28; D, 18.55)
side chain atoms	22.17 (A, 22.82; B, 21.72; C, 21.96; D, 22.18)
ligand atoms	29.39
water atoms	29.91
Ramachandran plot	
favored region	1183 (98.3%)
allowed region	21 (1.7%)

[a]Values in parentheses are for the outer shell.

asymmetric unit, the Matthews coefficient was calculated to be 2.36 Å^3 Da^{-1}, which corresponds to a solvent content of 47.9%.

Structure Determination and Refinement. The structure of BTUO in the complex with 8-azaxanthine has been determined by molecular replacement techniques. The initial phase was solved using the model of PDB entry 1J2G as a search probe. The MR solution was readily obtained and rebuilt using ARP/wARP.[18] The rebuilt model was then refined against the 1.75 Å data of the crystal using PHENIX.[19] Each round of refinement was alternated with a round of manual rebuilding using COOT,[20] and the refinement progress was monitored by tracking decreases in R_{cryst} and R_{free}. After several rounds of refinement, the electron density from the $|F_o| - |F_c|$ map depicted a clear density for 8-azaxanthine. The four subunit molecules in the asymmetric unit could be superimposed upon each other with a root-mean-square deviation (rmsd) for the Cα atoms of <0.38 Å, so that the refined overall structure was similar from monomer to monomer except at some crystal contact interfaces. Statistics for the refinement are listed in Table 1. The final coordinates were deposited in the Protein Data Bank as entry 3WLV.

Site-Directed Mutagenesis. Site-specific mutagenesis was conducted on BTUO at R298 by using the QuikChange site-directed mutagenesis kit (Stratagene) according to the manufacturer's protocols. The following primer pairs were used: forward (5′-GGGAAAGTATACACAGAACCGGAACCGCCATATG) and reverse (5′-CATATGGCGGTTCCGGTTCTGTGTATACTTTCCC). The R298E mutation was checked by sequencing with an ABI PRISM 377 DNA sequencer (Applied Biosystems). The mutant enzyme was overproduced and purified in the same way as the wild-type enzyme.

RESULTS

Sulfate-Induced Thermal Stabilization Observed via the Thermal Shift Assay. A fluorescent thermal shift assay was used to compare the effects of various sodium salts on the thermal stability of BTUO. This assay allows the protein melting curves for a number of protein samples to be monitored in multiwell plates, which greatly lowers the volume and protein requirements.[13,21,22] Figure 1 shows examples of thermal unfolding curves plotted as a function of temperature in the absence or presence of various sodium salts at 0.8 M. Although the resulting curve shape precludes strict interpretation of a two-state unfolding model, measurement of the melting curve using the same conditions with and without sodium salt allowed us to reproducibly determine the protein denaturation temperature midpoint (T_d) and to characterize the effect of different anions on protein thermal stability. Without salt additives, a T_d value for thermal denaturation was 68.6 °C, and the T_d values increased according to the anion's rank order in the Hofmeister series (Table 2). The presence of 0.8 M sodium sulfate increased the T_d value to 77.5 °C, which was the largest effect among the sodium salts investigated. Notably, the net height of the BTUO unfolding curves decreased by only 7% in the presence of 0.8 M Na_2SO_4, because the solution became slightly cloudy during heat denaturation. For other anions, the solutions became opaque but not cloudy. Such a phenomenon appears to be related to

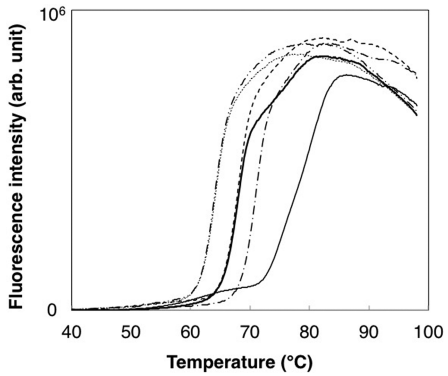

Figure 1. Denaturation profiles of BTUO in the presence of various salts: (thick solid) blank, (thin solid) 0.8 M Na_2SO_4, (dashed−dotted) CH_3COONa, (dashed) NaCl, (dashed−double dotted) $NaNO_3$, and (dotted) NaBr.

Table 2. Wild-Type BTUO T_d Values Determined Using the Thermal Shift Method (n = 4)

salt	T_d (°C)
free	68.6 ± 0.0$_5$
0.8 M NaBr	64.5 ± 0.0$_3$
0.8 M $NaNO_3$	64.5 ± 0.1
0.8 M NaCl	68.4 ± 0.1
0.8 M CH_3COONa	71.4 ± 0.0$_6$
0.8 M Na_2SO_4	77.5 ± 0.1

dx.doi.org/10.1021/bi500137b | Biochemistry 2014, 53, 3879−3888

the specific effect of sulfate salt, as similar results were also observed for salt-induced stabilization of ribonuclease A.[23]

The irreversible losses of enzyme activity during 30 min incubations at various temperatures were also determined at various Na_2SO_4 concentrations. The transition temperature at which the enzyme retains 50% of its initial activity ($T_{1/2}$) was 68 °C. The presence of 0.8 M Na_2SO_4 allowed a significant enhancement of the thermal stability such that the $T_{1/2}$ was 77 °C. The observed $T_{1/2}$ values closely corresponded to those from the thermal shift assay. In the meantime, the maximal reaction rate of the enzyme was not fundamentally affected until the sulfate salt concentration reached 1.2 M.

Salt-induced changes in T_d values were then evaluated by varying the concentration of three sodium salts with different anions (Na_2SO_4, CH_3COONa, and NaCl) and measuring the effects with a fluorescent thermal shift assay (Figure 2). All

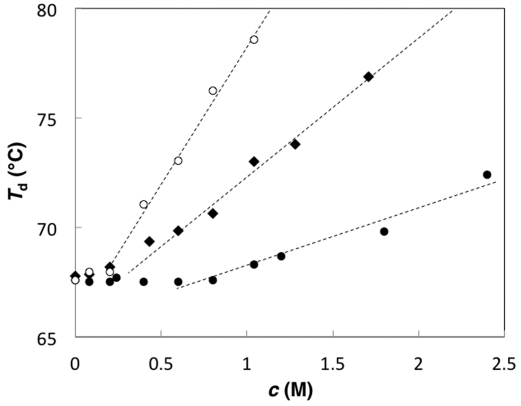

Figure 2. Salt concentration dependence of BTUO T_d values. Thermal shift assays were conducted at a protein concentration of 1 mg/mL and a heating rate of 0.8 K/min. Samples containing Na_2SO_4 (○), CH_3COONa (◆), and NaCl (●) were examined.

three plots showed a common feature in that the T_d values were approximately constant at lower salt concentrations (<0.2−0.6 M) and then rose in a linear fashion as the salt concentration increased. Such a threshold of salt concentration at which the linear plot slope increases has not been previously observed in corresponding plots for other proteins.[24−27] The T_d thresholds decreased in the following order: NaCl > CH_3COONa > Na_2SO_4. The plot slopes increased in the following order: NaCl < CH_3COONa < Na_2SO_4.

Differential Scanning Calorimetry at Various Sodium Sulfate Concentrations. DSC experiments were conducted to further investigate the effect of various Na_2SO_4 concentrations (0−1.0 M) on the thermal unfolding of BTUO. Borate buffer (pH 8.5) was used in DSC measurements to prevent turbidity. DSC curves of 2.7 mg/mL (18 μM) enzyme were obtained at a scanning rate of 1 K/min. In the absence of Na_2SO_4, the DSC thermogram profile had two distinct transition peaks: the first peak A and the second peak B, demonstrating that the BTUO thermal unfolding process has at least two distinct steps. Figure 3 shows the effect of Na_2SO_4 on BTUO thermal stabilization. The $T_{p,A}$ and $T_{p,B}$ values slightly decreased in the presence of low Na_2SO_4 concentrations (<0.2 M). As the concentration increased from 0.2 to 1.0 M, remarkable shifts to higher temperatures were observed for peak A but the second peak temperature, $T_{p,B}$, remained largely unaffected. At Na_2SO_4 concentrations of >0.8 M, peak A overlapped with peak B around 90 °C.

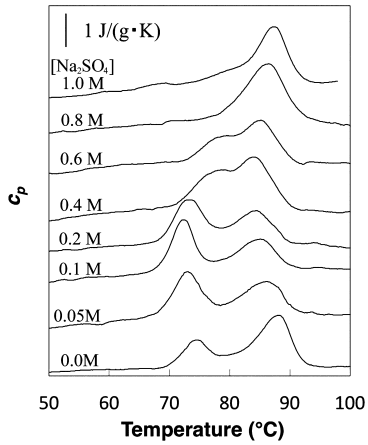

Figure 3. Differential scanning calorimetry thermograms of BTUO as a function of Na_2SO_4 concentration. The sample solution contained 2.7 mg/mL protein, 50 mM sodium borate (pH 8.5), and Na_2SO_4 as the salt. The spectra shown in the figure were recorded at the following Na_2SO_4 concentrations: 0, 0.05, 0.1, 0.2, 0.4, 0.6, 0.8, and 1.0 M.

Figure 4A shows DSC thermograms for 0.41−4.1 mg/mL BTUO in 50 mM sodium borate buffer at pH 8.5. As the enzyme concentration increased from 0.41 to 4.1 mg/mL, the maximal temperature of peak A ($T_{p,A}$) shifted to higher temperatures, but again no shift in peak B ($T_{p,B}$) was observed. The specific temperature shift of peak A suggested that the protein unfolding process at $T_{p,A}$ is related to BTUO subunit dissociation.[16] When the statistics of the fit to eq 2 were calculated, all DSC scans could be fit well to subunit dissociation coupled to the unfolding of the tetramer into two dimers. Figure 4B shows an example of the calculated baseline and baseline-subtracted fits at two peaks, where $T_{p,A}$ is given as 72.0 °C and $T_{p,B}$ is 87.6 °C.

Size Exclusion Chromatography Analysis of Subunit Composition. The subunit composition of BTUO was analyzed by SEC using a SuperSW3000 SEC column. As shown in Figure 5A, two sharp peaks were observed: the higher peak at 8.5 min had an elution volume consistent with the BTUO tetramer, while the lower peak at 12.7 min was assigned as a BTUO homodimer. This result was supported by native PAGE analysis, which was used to investigate the dissociation of *Bacillus fastidiosus* urate oxidase into two dimers under low-ionic strength conditions.[28] Thus, the SEC profile suggested that, under low-ionic strength conditions, the tetrameric enzyme dissociates into two dimers. To estimate dissociation constants K_d, the plots according to eq 4 were constructed using the degrees of association, Z, which were calculated from the peak areas of the tetramer and the dimer. Figure 4B shows that linear plots were obtained from the samples in the absence and presence of 0.8 M Na_2SO_4. Although the K_d values were difficult to determine quantitatively because of the low quantitation limit for the dimer, the presence of the sulfate salt significantly increased the slope of the plot, and it was suggested that the addition of the sulfate salt promoted the assembly of the dimers into the tetramer.

BTUO samples after a 1 min heat treatment at various temperatures were also analyzed by SEC. Without Na_2SO_4, the magnitude of the peak for the tetramer gradually decreased above 65 °C (Figure 5C,D). Comparatively, the samples containing 0.8 M Na_2SO_4 retained the tetramer after heat denaturation at 70 °C, and the magnitude of the peak abruptly

dx.doi.org/10.1021/bi500137b | *Biochemistry* 2014, 53, 3879−3888

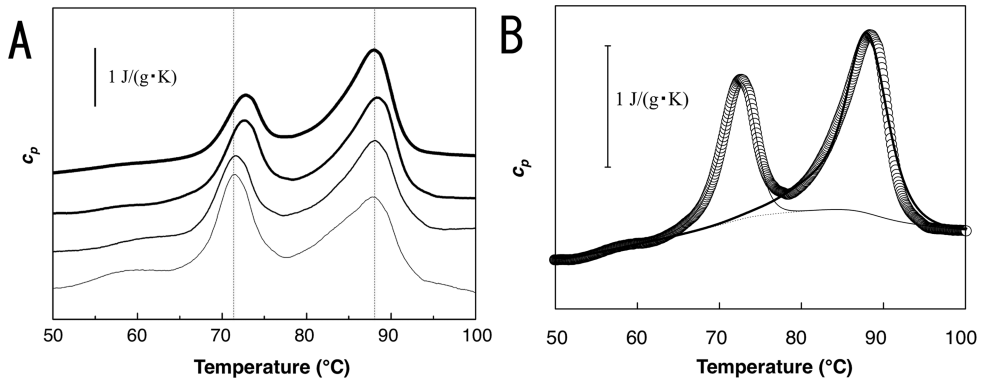

Figure 4. (A) DSC thermograms as a function of protein concentration. The thermograms shown in the figure were collected at the following protein concentrations: 0.41 (thin line), 0.61, 3.0, and 4.1 mg/mL (thick line). (B) DSC scan of BTUO in the absence of Na_2SO_4. The data points are shown as empty circles. The fits of the data to the sequential two-state model of eq 2 are indicated by thin (peak A), thick (peak B), and dotted (baseline) lines.

decreased above 70 °C. The trend toward decreased tetramer amounts was paralleled by the percentages of BTUO tetramers calculated from the DSC curves according to eq 2, particularly in the absence of Na_2SO_4. In the presence of 0.8 M Na_2SO_4, there was a significant temperature difference between the calculated line and the plot obtained from SEC analysis, probably because of a small filtration loss of the precipitate by partial salting out. Nevertheless, the amount of tetramer remaining after the heat treatment was definitely increased by the presence of Na_2SO_4. As a result, high Na_2SO_4 concentrations were shown to structurally and thermally stabilize BTUO tetramer assembly.

Structural Analysis of BTUO by X-ray Crystallography. The crystal structure of thermophilic BTUO in the presence of K_2SO_4 was determined in complex with the competitive inhibitor 8-azaxanthine at 1.75 Å resolution. The crystal structure of the tetramer molecule in the asymmetric unit exhibits four identical subunits enclosing a tunnel, with each subunit composed of two tandem tunneling-fold motifs[29] (Figure 6A), which is similar to mesophilic uricase from *Asperigillus flavus* (AFUO, PDB entry 1R51)[30] and that from *Arthrobacter globiformis* (AGUO, PDB entry 1VAY). The sequence of BTUO is 26.3 and 25.6% identical to those of AFUO and AGUO, respectively, and all catalytic residues in the active site are conserved completely. The central tunnel structure is built by stacking of two antiparallel β-barrels of subunit dimers, and the active site is located at the subunit interface in the dimer β-barrel. Superposition of the 8-azaxanthine complex of thermophilic BTUO onto that of mesophilic AFUO using GASH[31] (Figure 6B) revealed a rmsd of 1.68 Å for 227 Cα atoms overall, 6 times higher than the rmsd averaged among the four subunit chains of BTUO (0.28 Å). Major structural differences were concentrated in four peripheral loops, and we referred to two characteristic loops at the tetrameric interface as interface loop I (residues 125−145) and interface loop II (residues 277−300). Both loops extend to the neighboring dimer ring and are involved in forming the tetramer structure.

Figure 6C shows the structure around interface loop II of subunit C, which is placed at the interface between subunits A and B. In the N-terminal region of the loop, a bound sulfate anion formed a symmetrical intersubunit salt bridge with the Arg298 residues of subunits A and C, and its structure was well-defined in the electron density map. Arg298 also makes a bifurcated hydrogen bond with Asp280 of subunit A. Table 3 shows hydrogen bond pairs around interface loop II as estimated using PDBePISA.[32] In the carboxy-terminal region of the loop, the short Lys292−Glu296 strand of subunit C forms six hydrogen bonds with the antiparallel Phe17−Thr21 β-strand of subunit B. As a result, the bound sulfate can lock the tunnel dimer via interface loop II protruding from another tunnel dimer. The loop contained the highest-*B* factor region (residues 281−292). The averaged main chain *B* factor of the region was 35.0 Å,^{2} which is ∼2-fold higher than that of the overall main chain (18.4 Å^2), and suggests that this loop may play a role as a hinge between subunits A and B that could participate in the opening−closing motion of the active site cleft at the subunit interface.

Mutagenesis Studies of the Role of Arginine 298 in Thermal Stabilization Induced by Sulfate Binding. The results from the thermal and structural analyses described above suggest that the thermal stability of the tetramer is controlled by the sulfate binding to Arg298. To confirm this assumption, site-directed mutagenesis to substitute glutamate for Arg298 was conducted, and kinetic and calorimetric analyses of the R298E mutant were performed.

The kinetic parameters of the BTUO mutant are summarized in Table 4. Although Arg298 is located in interface loop II apart from the active site, the R298E substitution resulted in a mutant enzyme with a k_{cat} value that was reduced by 2.4-fold and a K_m value increased by 4-fold. Following the addition of 1.2 M Li_2SO_4 or Na_2SO_4, the R298E mutant remained fully active while the K_m value of wild-type BTUO increased by 3.4- or 5.4-fold. These results suggest that the sulfate binding at the Arg298 lowered the affinity for the substrate, and its substitution with Glu caused the loss of the symmetrical interaction with a sulfate. The shielding effect by the high concentration of salt might reduce the affinity for the substrate. However, R298E shows no significant changes in the K_m values in the presence of 1.2 M sulfate salt. The results may imply that the sulfate binding at Arg298 induces a loss of conformational flexibility that allows the substrate to bind to the active site properly.

The DSC transition curve of the R298E mutant showed profound changes (Figure 7). In the absence of Na_2SO_4, the DSC profile of the mutant showed an apparent single transition peak (Figure 7A). When the Na_2SO_4 concentration was increased above 0.2 M, the peak shifted slightly to a higher temperature, and when the concentration was above 0.6 M, a shoulder appeared on the higher-temperature side of the peak

dx.doi.org/10.1021/bi500137b | *Biochemistry* 2014, 53, 3879−3888

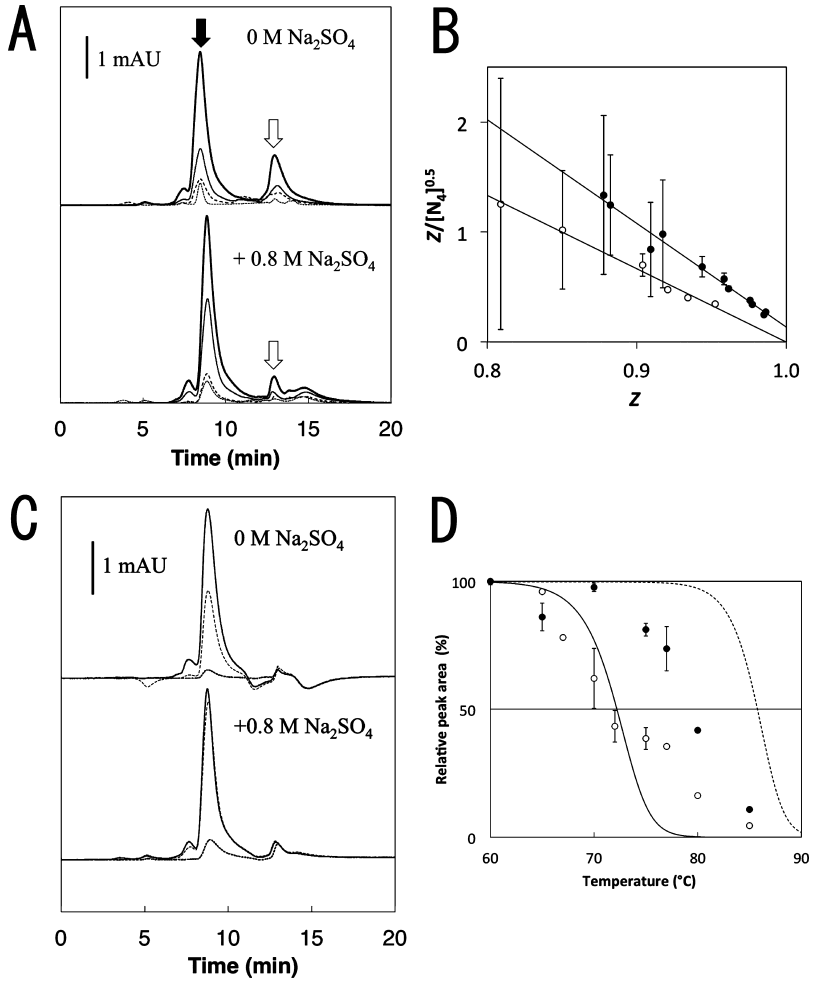

Figure 5. Size exclusion chromatographic analyses of BTUO. (A) The effect of sulfate salt on the enzyme subunit composition was analyzed. Samples [protein concentrations of 0.41 (dotted), 0.61 (dashed), 1.2 (thin solid), and 4.1 mg/mL (thick solid)] were prepared in the absence or presence of 0.8 M Na_2SO_4. To analyze the effect of low-ionic strength conditions, 50 mM sodium phosphate buffer (pH 7.0) was used for the SEC analysis of Na_2SO_4-free samples. The black and white arrows represent the peaks of the tetramer and dimer, respectively. (B) Estimation of the apparent dissociation constant for the BTUO tetramer, K_d based on eq 4. Empty and filled circles represent the data for samples in the absence and presence of 0.8 M Na_2SO_4, respectively. The degrees of association, Z, were calculated from the peak areas of the tetramer and the dimer (the BTUO concentrations ranged from 0.08 to 2.36 mg/mL). Error bars represent the standard errors between two different experiments. The fits of the data to eq 4 are indicated by thin lines. (C) In the absence or presence of 0.8 M Na_2SO_4, soluble BTUO after thermal denaturation for 1 min at the specified temperatures was analyzed by SEC. SEC profiles of samples denatured at 60 (thick), 75 (dashed), and 85 °C (dotted) are shown. (D) Plot of the relative area of the tetramer peak at the respective temperatures. The empty and filled circles represent the data for samples in the absence and presence of 0.8 M Na_2SO_4, respectively. Error bars represent the standard errors between different experiments (n = 3). The estimated percentages of BTUO tetramers were calculated from the DSC curves analyzed according to eq 2, and the values in the absence and presence of 0.8 M Na_2SO_4 are represented as solid and dashed lines, respectively.

(in the presence of 0.8 M Na_2SO_4, the $T_{p,A}$ and $T_{p,B}$ values of the mutant enzyme reached 75.1 and 81.1 °C, respectively). When the statistics of the fit were calculated assuming the model represented in eq 2, the DSC scans fit well (Figure 7C). These analyses revealed that the mutation markedly reduced the magnitudes of the second transition peaks and lowered the $T_{p,B}$. At concentrations ranging from 0 to 0.6 M, the $T_{p,B}$ value of R298E was 12−16 °C lower than that of the wild-type enzyme (Figure 7B), while the decrease in the $T_{p,A}$ of the mutant enzyme was between 2 and 7 °C of the $T_{p,A}$ of the wild-type enzyme. The glutamate substitution reduced the dependency of the increase in $T_{p,A}$ values on Na_2SO_4 concentration.

DISCUSSION

A high concentration of sulfate salt critically induced the thermal stabilization of BTUO, as shown by analyses of the thermal shift in fluorescence, the residual activity assay, DSC, and SEC. These analyses revealed several unique features of the salt effect. (1) Sulfate salts strongly induce thermal stabilization. (2) An unusual threshold of the salt concentration appeared in the anion-induced thermal stabilization as shown in Figure 2. (3) The DSC curve of wild-type BTUO at low Na_2SO_4 salt concentrations showed a two-step transition of unfolding, with the initial unfolding step chiefly related to the salt-induced thermal stabilization. (4) Sulfate salts prevented the tetramer from dissociating into two homodimers and stabilized the assembly of the subunits. These characteristics suggest a previously unknown mechanism of salt-induced thermal stabilization.

The two distinct peaks in the DSC curve demonstrated that at least two unfolding steps occurred during the heat denaturation. As the concentration of protein increased, the

dx.doi.org/10.1021/bi500137b | Biochemistry 2014, 53, 3879−3888

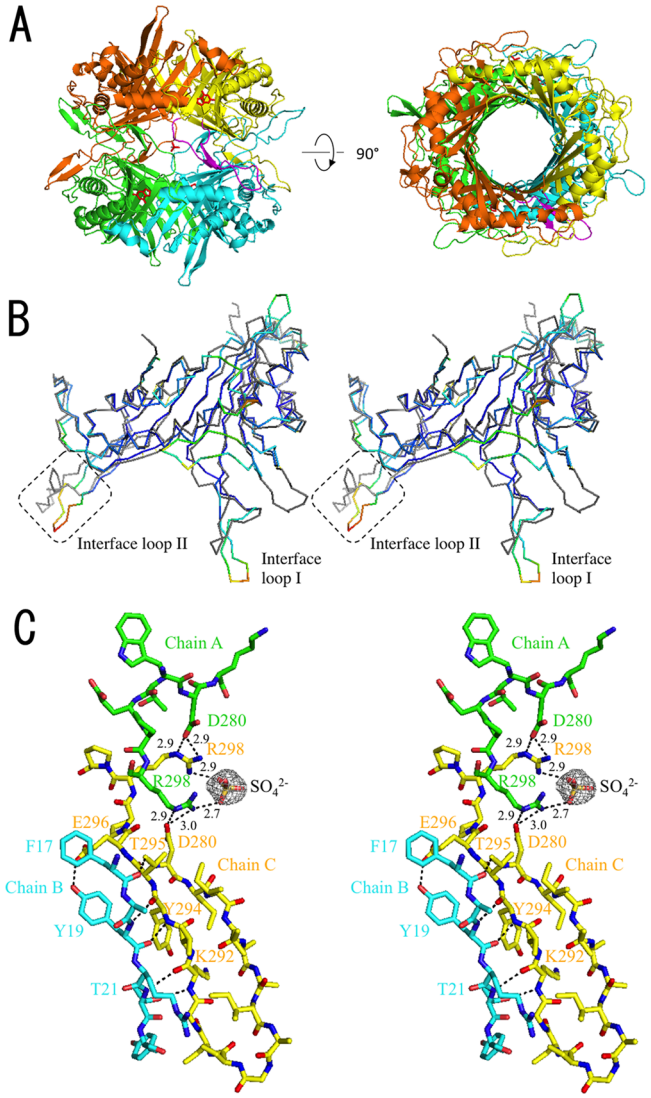

Figure 6. Structures of BTUO in complex with 8-azaxanthine. (A) Side and top views of a schematized model of the BTUO tetramer. Subunits A–D are colored green, cyan, yellow, and orange, respectively. Bound ligands are shown as red stick models. Interface loop II (residues 277–300) of subunit C is colored magenta. Panel A was prepared using PyMOL.[33] (B) Comparison of BTUO and AFUO subunit structures. The BTUO molecule is colored according to its temperature factor, from dark blue for a low *B* factor to red for a high *B* factor. (C) Estimated hydrogen bonds are drawn as dashed lines, and numbers show contact distances between the nitrogen atoms of Arg298 and the oxygen atoms of SO_4^{2-} or Asp280. SIGMAA-weighted $|F_o| - |F_c|$ omit electron density maps for sulfate anion. The map is contoured at 3σ.

melting temperature $T_{p,A}$ shifted to a higher temperature, implying that the subunit dissociation was related to the first unfolding step. Meanwhile, the $T_{p,B}$ of peak B remained almost constant, regardless of the protein concentration used in the experiment. To analyze the two-step unfolding of BTUO, we presumed a simple model expressed by eq 2, which is simple and able to explain the finding that dissociation into homodimers was always followed by the next unfolding step. Figure 4B shows the DSC experimental curve and the best fits to eq 2. Despite the simplifying assumption of reversibility, the main features of the thermal profile are represented well.

Table 3. Predicted Hydrogen Bond Pairs around Interface Loop II[a]

interface loop II	bond length (Å)	bonding partner
C, Asp280 OD2	3.21	A, Arg298 NE
C, Asp280 OD2	3.10	A, Arg298 NH2
C, Arg298 NE	3.26	A, Asp280 OD2
C, Arg298 NH2	3.04	A, Asp280 OD2
C, Lys292 N	3.01	B, Thr21 OG1
C, Tyr294 N	2.84	B, Tyr19 O
C, Thr295 OG1	2.63	B, Phe17 O

[a]To specify each atom of the hydrogen bond donors and acceptors, the chain name, residue name, residue number, and atom name are given.

Zhao et al. reported that the urate oxidase from *B. fastidiosus*, a homologue of BTUO (amino acid sequence identity of 57%), dissociated into inactive homodimers in low-ionic strength solutions.[28] This dissociation into dimers was also observed for BTUO (Figure 5A). Although the BTUO dimer structure has remained unknown, the solvation energies of the dimer interfacing residues estimated by PISA[34] are −29.2 kcal/mol between the subunits present in the *β*-barrel (chain A-B/C-D) and −24.6 kcal/mol for another possible dimer (chain B-C/D-A). The energy difference mainly results from the formation of hydrogen bonds between the strands in the *β*-barrel. On the basis of the PISA analysis, the formation of the *β*-barrel dimer in the first unfolding step seems probable, but further study is required to reveal the dimer structure.

The heat treatment experiment showed that high concentrations of Na_2SO_4 contributed to the stable maintenance of the homotetramer structure (Figure 5C,D). These results suggested that the salt-dependent stabilization of the tetramer structure was paralleled by an increase in thermal stability. In salt-induced thermal stabilization of *Methanopyrus kandleri* formyltransferase, association of subunit monomers was reported.[35] Although this salt-induced oligomerization conferred a high thermal stability on the formyltransferase, no evidence concerning the identity of the bound ion species that was responsible for the thermal stabilization was provided. However, the unusual threshold of Na_2SO_4 concentration in the thermal stabilization of BTUO (Figure 2) indicated the presence of a specific binding site for sulfate in this enzyme, which prompted our exploration of the sulfate binding site using X-ray crystallography. In the BTUO crystal structure at 1.75 Å resolution, the binding site of a sulfate anion was found between the two adjacent Arg298 residues in interface loop II that had a 2-fold axis of symmetry relationship.

The substitution of Arg298 with Glu was originally designed to inhibit binding of the sulfate anion to BTUO, which was expected to diminish the thermal stability provided by the presence of the sulfate and to destabilize the native state of the enzyme because of the electrostatic repulsion between Glu298 and Asp280 under low-ionic strength conditions. In fact, the $T_{p,A}$ value of the R298E enzyme was always 2–7 °C lower than that of the wild type, and the slope of the plot of $T_{p,A}$ versus Na_2SO_4 concentration decreased (Figure 7B). These results suggested that the network of charged hydrogen bonds via the bound sulfate contributed to the thermal stabilization of BTUO. A possible explanation for the sulfate-induced thermal stabilization of R298E that persisted is the stabilization of the tetramer assembly by the Hofmeister effect. An increase in ionic charge density (the ionic charge per unit ionic volume) was

dx.doi.org/10.1021/bi500137b | *Biochemistry* 2014, 53, 3879–3888

Table 4. BTUO Kinetic Parameters at 37 °C

	50 mM borate buffer at pH 8 (n = 3)		with 1.2 M Li_2SO_4 (n = 2)		with 1.2 M Na_2SO_4 (n = 3)	
	k_{cat} (s^{-1})	K_m (μM)	k_{cat} (s^{-1})	K_m (μM)	k_{cat} (s^{-1})	K_m (μM)
wild type	2.4 ± 0.3	14 ± 1	2.2 ± 0.3	47 ± 13	2.3 ± 0.5	75 ± 5
R298E	1.0 ± 0.1	59 ± 2	0.9 ± 0.1	66 ± 5	0.8 ± 0.1	72 ± 3

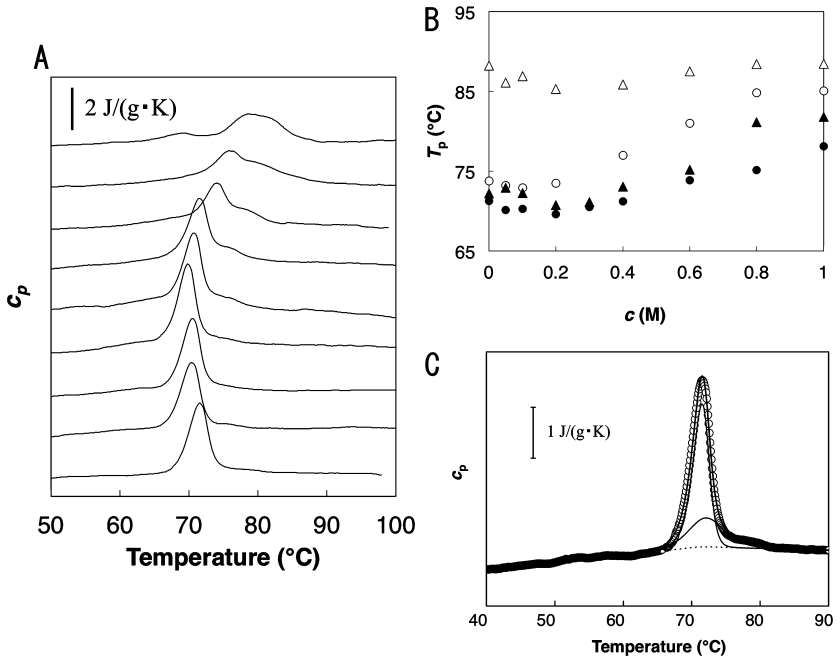

Figure 7. DSC thermograms of mutant R298E as a function of Na_2SO_4 concentration. The sample solution contains 2.7 mg/mL protein, 50 mM sodium borate (pH 8.5), and Na_2SO_4 as a salt. (A) The thermograms shown in the figure were collected at Na_2SO_4 concentrations of 0, 0.05, 0.1, 0.2, 0.3, 0.4, 0.6, 0.8, and 1.0 M. (B) The changes in T_p values were calculated from the DSC thermograms. Empty circles and triangles are $T_{p,A}$ and $T_{p,B}$ values, respectively, of the wild-type enzyme, and filled circles and triangles represent those of the R298E mutant, respectively. (C) DSC scan of the R298E mutant in the absence of Na_2SO_4. The data points are shown as empty circles. The fits of the data to the sequential two-state model of eq 2 are indicated by thin lines.

suggested to amplify the hydrophobic interaction between nonpolar solutes.[36,37]

Unexpectedly, however, the thermal unfolding process of R298E was mostly affected at the second unfolding step (Figure 7A). The area of the transition peak for this second step decreased, as did the $T_{p,B}$ values. One possible explanation is that the unfolding process was changed to a single-step transition to the completed denatured state. At higher concentrations of Na_2SO_4 (>0.6 M), the $T_{p,B}$ of the R298E mutant increased remarkably compared with $T_{p,A}$ and the second peak clearly appeared in the DSC curve (Figure 7A). Moreover, even at 0 M Na_2SO_4, the asymmetrical DSC curve of R298E was fit to the two-step unfolding model of eq 2 better than the single-step model. The hypothesis of the one-step unfolding suggests the inconsistency with these experimental results. Therefore, the two-step unfolding model may be valid for the explanation of the R298E heat denaturation. According to eq 2, the significant decrease in $T_{p,B}$ of R298E implies that the mutation primarily promoted the unfolding of U_2 and had a relatively weak effect on the unfolding of the native tetramer N_4. The mechanism of R298E destabilization has remained unknown, and further studies of the substitution of this residue are in progress and will be reported elsewhere.

Binding of sulfate anions on the surface of a protein is a familiar phenomenon. Sulfate binding can provide thermodynamic stabilization of small proteins,[25,38] providing evidence of the stabilizing effect of surface-exposed electrostatic interactions and regular charge networks. Solvent-exposed salt bridges are generally expected to have a marginal effect on the thermal stability of large proteins. The effect of salt additives (e.g., ammonium sulfate) on large proteins has been frequently explained by the Hofmeister effect on protein stability.[36,39,40] An ion's influence on protein stability has been proposed to be caused in part by the shielding of surface charges by bulk ion species and their acting as osmolytes that affect the bulk properties of water. Recently, special attention was given to direct ion−macromolecule interactions as well as interactions with water molecules in the first hydration shell of the macromolecule.[41] The Hofmeister effect is thought mainly to result from direct ion interactions rather than changes in the bulk water structure.

Our findings reveal that binding of a sulfate anion to BTUO promoted remarkable thermal stabilization via the formation of a polar hydrogen bonding network on the protein surface. The structure of this bonding network will provide information for the rational design to enhance and control protein thermal stability.

■ ASSOCIATED CONTENT

Accession Codes

The atomic coordinates and structure factors have been deposited as PDB entry 3WLV.

AUTHOR INFORMATION

Corresponding Author

*Department of Bioscience, Fukui Prefectural University, Fukui 910-1195, Japan. E-mail: hibi@fpu.ac.jp. Telephone: +81 (776) 61-6000. Fax: +81 (776) 61-6015.

Present Addresses

[‖]T.N.: Eidai Co. Ltd., Eidai-cho, Tsuruga, Fukui 914-0047, Japan.

[⊥]Y.N.: Department of Life Science, Setsunan University, 17-8 Ikedanaka-machi, Neyagawa, Osaka 572-8508, Japan.

Author Contributions

T.H. was the Principal Investigator and conducted X-ray crystallography and enzyme kinetics. T.N. conducted purification and kinetic analysis of the enzyme and crystallization screening. Y.H. conducted chromatographic analysis and X-ray crystallography. Y.N. conducted genetic engineering and enzyme purification. H.F. conducted calorimetry. T.I. conducted X-ray crystallography.

Funding

This work was supported by a Grant-in-Aid for Scientific Research (12660099) from the Japan Society for the Promotion of Science.

Notes

The authors declare no competing financial interest.

ACKNOWLEDGMENTS

We thank the staff at the Photon Factory for providing data collection facilities and support. The synchrotron radiation experiments were performed at beamline NW-12A (Proposal 2011G674). We thank Prof. H. Yamaguchi (Kwansei Gakuin University) for generous advice and support.

ABBREVIATIONS

BTUO, urate oxidase from *Bacillus* sp. TB-90; AFUO, urate oxidase from *A. flavus*; AGUO, urate oxidase from *Ar. globiformis*; CCD, charge-coupled device; PDB, Protein Data Bank; rmsd, root-mean-square deviation; DSC, differential scanning calorimetry; SEC, size exclusion chromatography.

REFERENCES

(1) Kageyama, N. (1971) A direct colorimetric determination of uric acid in serum and urine with uricase-catalase system. *Clin. Chim. Acta 31*, 421−426.

(2) Brant, J. M. (2002) Rasburicase: An innovative new treatment for hyperuricemia associated with tumor lysis syndrome. *Clinical Journal of Oncology Nursing 6*, 12−16.

(3) Lotfy, W. A. (2008) Production of a thermostable uricase by a novel *Bacillus thermocatenulatus* strain. *Bioresour. Technol. 99*, 699−702.

(4) McCarthy, M., and Johnson, D. B. (1977) Urate oxidase immobilization on elastin. *Biotechnol. Bioeng. 19*, 599−603.

(5) Zhang, C., Yang, X., Feng, J., Yuan, Y., Li, X., Bu, Y., Xie, Y., Yuan, H., and Liao, F. (2010) Effects of modification of amino groups with poly(ethylene glycol) on a recombinant uricase from *Bacillus fastidiosus*. *Biosci., Biotechnol., Biochem. 74*, 1298−1301.

(6) Tan, Q. Y., Wang, N., Yang, H., Zhang, L. K., Liu, S., Chen, L., Liu, J., Zhang, L., Hu, N. N., Zhao, C. J., and Zhang, J. Q. (2010) Characterization, stabilization and activity of uricase loaded in lipid vesicles. *Int. J. Pharm. 384*, 165−172.

(7) Kim, K., Park, J., and Rhee, S. (2007) Structural and functional basis for (S)-allantoin formation in the ureide pathway. *J. Biol. Chem. 282*, 23457−23464.

(8) Nishiya, Y., Hibi, T., and Oda, J. i. (2000) The full DNA sequence of the gene encoding the diagnostic enzyme *Bacillus* uricase. *Journal of Analytical Bio-Science 23*, 443−446.

(9) Yamamoto, K., Kojima, Y., Kikuchi, T., Shigyo, T., Sugihara, K., Takashio, M., and Emi, S. (1996) Nucleotide Sequence of the Uricase Gene from *Bacillus* sp. TB-90. *J. Biochem. 119*, 80−84.

(10) Von Hippel, P. H., and Schleich, T. (1969) Ion effects on the solution structure of biological macromolecules. *Acc. Chem. Res. 2*, 257−265.

(11) Edelhoch, H. (1967) Spectroscopic determination of tryptophan and tyrosine in proteins. *Biochemistry 6*, 1948−1954.

(12) Pace, C. N., Vajdos, F., Fee, L., Grimsley, G., and Gray, T. (1995) How to measure and predict the molar absorption coefficient of a protein. *Protein Sci. 4*, 2411−2423.

(13) Niesen, F. H., Berglund, H., and Vedadi, M. (2007) The use of differential scanning fluorimetry to detect ligand interactions that promote protein stability. *Nat. Protoc. 2*, 2212−2221.

(14) Müller, M., and Møller, K. M. (1969) Studies on some enzymes of purine metabolism in the amoebae *Chaos chaos* and *Amoeba proteus*. *C. R. Trav. Lab. Carlsberg 36*, 463−497.

(15) Privalov, P. L., and Potekhin, S. A. (1986) Scanning microcalorimetry in studying temperature-induced changes in proteins. *Methods Enzymol. 131*, 4−51.

(16) Sturtevant, J. M. (1987) Biochemical Applications of Differential Scanning Calorimetry. *Annu. Rev. Phys. Chem. 38*, 463−488.

(17) Otwinowski, Z., and Minor, W. (1997) Processing of X-ray diffraction data collected in oscillation mode. *Methods Enzymol. 276*, 307−326.

(18) Langer, G., Cohen, S. X., Lamzin, V. S., and Perrakis, A. (2008) Automated macromolecular model building for X-ray crystallography using ARP/wARP version 7. *Nat. Protoc. 3*, 1171−1179.

(19) Adams, P. D., Afonine, P. V., Bunkoczi, G., Chen, V. B., Davis, I. W., Echols, N., Headd, J. J., Hung, L. W., Kapral, G. J., Grosse-Kunstleve, R. W., McCoy, A. J., Moriarty, N. W., Oeffner, R., Read, R. J., Richardson, D. C., Richardson, J. S., Terwilliger, T. C., and Zwart, P. H. (2010) PHENIX: A comprehensive Python-based system for macromolecular structure solution. *Acta Crystallogr. D66*, 213−221.

(20) Emsley, P., and Cowtan, K. (2004) Coot: Model-building tools for molecular graphics. *Acta Crystallogr. D60*, 2126−2132.

(21) Carver, T. E., Bordeau, B., Cummings, M. D., Petrella, E. C., Pucci, M. J., Zawadzke, L. E., Dougherty, B. A., Tredup, J. A., Bryson, J. W., Yanchunas, J., Jr., Doyle, M. L., Witmer, M. R., Nelen, M. I., DesJarlais, R. L., Jaeger, E. P., Devine, H., Asel, E. D., Springer, B. A., Bone, R., Salemme, F. R., and Todd, M. J. (2005) Decrypting the biochemical function of an essential gene from *Streptococcus pneumoniae* using ThermoFluor technology. *J. Biol. Chem. 280*, 11704−11712.

(22) Lavinder, J. J., Hari, S. B., Sullivan, B. J., and Magliery, T. J. (2009) High-throughput thermal scanning: A general, rapid dye-binding thermal shift screen for protein engineering. *J. Am. Chem. Soc. 131*, 3794−3795.

(23) Ginsburg, A., and Carroll, W. R. (1965) Some Specific Ion Effects on the Conformation and Thermal Stability of Ribonuclease. *Biochemistry 4*, 2159−2174.

(24) Kaushik, J. K., and Bhat, R. (1999) A mechanistic analysis of the increase in the thermal stability of proteins in aqueous carboxylic acid salt solutions. *Protein Sci. 8*, 222−233.

(25) Makhatadze, G. I., Lopez, M. M., Richardson, J. M., III, and Thomas, S. T. (1998) Anion binding to the ubiquitin molecule. *Protein Sci. 7*, 689−697.

(26) Ramos, C. H., and Baldwin, R. L. (2002) Sulfate anion stabilization of native ribonuclease A both by anion binding and by the Hofmeister effect. *Protein Sci. 11*, 1771−1778.

(27) Tadeo, X., Pons, M., and Millet, O. (2007) Influence of the Hofmeister anions on protein stability as studied by thermal denaturation and chemical shift perturbation. *Biochemistry 46*, 917−923.

(28) Zhao, Y., Yang, X., Li, X., Bu, Y., Deng, P., Zhang, C., Feng, J., Xie, Y., Zhu, S., Yuan, H., Yu, M., and Liao, F. (2009) Reversible

inactivation of an intracellular uricase from *Bacillus fastidiosus* via dissociation of homotetramer into homodimers in solutions of low ionic strength. *Biosci., Biotechnol., Biochem. 73*, 2141−2144.
(29) Colloc'h, N., Poupon, A., and Mornon, J.-P. (2000) Sequence and structural features of the T-fold, an original tunnelling building unit. *Proteins: Struct., Funct., Bioinf. 39*, 142−154.
(30) Colloc'h, N., Hajji, M. E., Bachet, B., L'Hermite, G., Schiltz, M., Prangé, T., Castro, B., and Mornon, J.-P. (1997) Crystal structure of the protein drug urate oxidase-inhibitor complex at 2.05 Å resolution. *Nat. Struct. Biol. 4*, 947−952.
(31) Toh, H. (1997) Introduction of a distance cut-off into structural alignment by the double dynamic programming algorithm. *Comput. Appl. Biosci. 13*, 387−396.
(32) Xu, Q., Canutescu, A. A., Wang, G., Shapovalov, M., Obradovic, Z., and Dunbrack, R. L., Jr. (2008) Statistical analysis of interface similarity in crystals of homologous proteins. *J. Mol. Biol. 381*, 487−507.
(33) DeLano, W. L. (2002) *The PyMOL Molecular Graphics System*, DeLano Scientific, San Carlos, CA.
(34) Krissinel, E., and Henrick, K. (2007) Inference of macromolecular assemblies from crystalline state. *J. Mol. Biol. 372*, 774−797.
(35) Shima, S., Tziatzios, C., Schubert, D., Fukada, M., Takahashi, K., Ermler, U., and Thauer, R. K. (1998) Lyotropic-salt-induced changes in monomer/dimer/tetramer association equilibrium of formyltransferase from the hyperthermophilic *Methanopyrus kandleri* in relation to the activity and thermostability of the enzyme. *Eur. J. Biochem. 258*, 85−92.
(36) Baldwin, R. L. (1996) How Hofmeister ion interactions affect protein stability. *Biophys. J. 71*, 2056−2063.
(37) Collins, T., Meuwis, M. A., Gerday, C., and Feller, G. (2003) Activity, stability and flexibility in glycosidases adapted to extreme thermal environments. *J. Mol. Biol. 328*, 419−428.
(38) Merz, T., Wetzel, S. K., Firbank, S., Pluckthun, A., Grutter, M. G., and Mittl, P. R. (2008) Stabilizing ionic interactions in a full-consensus ankyrin repeat protein. *J. Mol. Biol. 376*, 232−240.
(39) von Hippel, P. H., and Wong, K. Y. (1964) Neutral Salts: The Generality of Their Effects on the Stability of Macromolecular Conformations. *Science 145*, 577−580.
(40) Broering, J. M., and Bommarius, A. S. (2005) Evaluation of Hofmeister effects on the kinetic stability of proteins. *J. Phys. Chem. B 109*, 20612−20619.
(41) Zhang, Y., and Cremer, P. S. (2006) Interactions between macromolecules and ions: The Hofmeister series. *Curr. Opin. Chem. Biol. 10*, 658−663.